

# On the applicability of Kerker preconditioning scheme to the self-consistent density functional theory calculations of inhomogeneous systems

Yuzhi Zhou,<sup>1,2</sup> Han Wang,<sup>2,3</sup> Yu Liu,<sup>1,2</sup> Xingyu Gao,<sup>1,2</sup> and Haifeng Song<sup>1,2</sup>

<sup>1</sup>*LCP, Institute of Applied Physics and Computational Mathematics,  
Beijing 100088, Peoples Republic of China*

<sup>2</sup>*Software Center for High Performance Numerical Simulation,  
Chinese Academy of Engineering Physics,  
Beijing 100088, Peoples Republic of China*

<sup>3</sup>*Institute of Applied Physics and Computational Mathematics,  
Beijing 100088, Peoples Republic of China*

(Dated: December 14, 2024)

## Abstract

Kerker preconditioner, which is based on the dielectric function of homogeneous electron gas, is designed to accelerates the self consistent field (SCF) density functional theory (DFT) based total-energy calculations. However, question regarding its applicability to the inhomogeneous systems still remains. In this paper, we propose a generalized Kerker preconditioning scheme which works well for the SCF calculations of inhomogeneous systems. Various numerical examples on metallic, insulating and metal-insulator hybrid systems prove the effectiveness and efficiency of our preconditioning model. In order to reach fast convergence, we find that it is crucial to have a correct description of the dielectric response around long wavelength limit.

## I. INTRODUCTION

Over the past few decades, the Kohn-Sham based density functional theory (DFT) calculation [1, 2] has evolved into one of the major *ab initio* approaches for predicting the electronic structures and related properties of matters. The computational kernal of the Kohn-Sham based DFT framework is to solve a tangible nonlinear eigenvalue problem replacing the original difficult many-body problem, first proposed by Kohn and Sham in the 1960s [2]. This nonlinear eigenvalue problem is usually solved by the self consistent field (SCF) iteration methods, which have proved to be quite reliable and efficient in most cases [3]. However, the well known "charge sloshing" problem occurs in the SCF loop as the dimension of the system gets large. The charge sloshing generally refers the long-wavelength oscillations of the output charge density due to some small changes in the input density during the iterations, and results in a slow convergence or even divergence [3–5] (while in some cases it might be referred to the oscillation between different local states of the d or f electrons [6] and we mainly focus on the discussion of the former situation in this paper). For a given number of total atoms, the charge sloshing and poor convergence are more prominent in the long-z slab systems, where one dimension of the unit cell is much longer than the other two's. On the other hand, investigating the properties of the surface and interface using DFT calculations has become a crucial subject in many scientific and technological fields, such as solid state physics, semiconductor processing, corrosion, and heterogeneous catalysis [7, 8]. Within the periodic boundary condition, a surface/interface is generally simulated by the long-z slab model. Generally speaking, such calculations also requires higher accuracy than the bulk calculations. Effective and efficient mixing schemes are therefore needed to speed up the convergence and suppress charge sloshing.

In view of improving mixing schemes, there are generally two aspects of consideration: (1) taking the information of previous iterations into account; (2) Reflecting the dielectric response of the system (better known as "precondintioning"). A practical mixing scheme implemented in the modern DFT code generally takes advantage of both. For the first aspect, Pulay and Broyden-like schemes are well established and among the most commonly used schemes [9, 10]. For the second aspect, Kerker in 1981 proposed that charge mixing could be preconditioned by a diagonal matrix in the reciprocal space. This matrix takes the form of inverse dielectric matrix derived from Thomas-Fermi model of homogeneous electron

gas [11]. As pointed out in many work (and we will briefly visit it again in the next section), the preconditioning matrix should be an approximation to the dielectric function of the system [3, 12, 13]. In this sense, the Kerker preconditioner is ideal for simple metals such as Na and Al in which the conduction electrons behave like free electrons. Moreover, for most metallic systems, the Kerker preconditioner is a good approximation since it describes the dielectric responses at long wavelength limit fairly well. This observation then raises a natural question: Can Kerker preconditioning technique be applied to the non-metallic systems and metal-insulator hybrid systems?

Many efforts have been devoted to develop effective preconditioning schemes: Kresse *et al.* suggests that within the Kerker scheme, a lower bound can be added to the model dielectric function for large insulating systems [3]. Raczkowski *et al.* use the Thomas-Fermi-von Weizsäcker equation to directly solve for the optimized mixing density in which process the full dielectric function is implicitly solved [12]; Shiihara *et al.* recast the Kerker preconditioning scheme in the real space for efficient SCF based real-space calculations [14]; Lin and Yang further proposed an elliptic preconditioner in the real space to better accommodates the SCF calculations of large inhomogeneous systems [15]; Ho *et al.* [16], Sawamura *et al.* [17] and Anglade *et al.* [18] adopt similar precondition schemes that take root in the computation of the exact dielectric matrix using the calculated eigenfunctions and eigenenergies.

In this paper, together with theoretical analysis and numerical examples, we show that Kerker preconditioning scheme can be generalized to accelerate the SCF based DFT calculations for metallic, insulating and metal-insulator hybrid systems. It is argued that under the framework of Thomas-Fermi model, with physically meaningful modifications, the Kerker preconditioner can work fairly well to the non-metallic systems: For perfect insulating system, a threshold parameter is introduced to capture the behaviour of dielectric responses at small reciprocal lattice vectors; For metal-insulator hybrid systems and insulators containing metal-like defect states, the idea of the "effective" metal-like electrons is introduced to parameterized the Thomas-Fermi wave vector in the preconditioner. Our generalized preconditioning technique requires easy modifications of the modern DFT packages, and is efficient and effective over a wide range of inhomogeneous systems. We also provide *a posteriori* indicator to monitor if the charge sloshing have been suppressed or not.

This paper is organized as follows: In Sec. II, we will review the mathematical framework

of Pulay mixing scheme and its interconnection the preconditioner. In Sec. III, we will revisit the Kerker preconditioner and Thomas-Fermi model with their extension to the non-metallic systems. Our scheme will be examined by several numerical examples. A further discussion on the essence of this preconditioning technique and parametrization strategy will be given in Sec IV. Finally, concluding remarks will be presented in the last section.

## II. MATHEMATICAL FRAMEWORK

### A. Simple mixing and preconditioning

Finding the solution of the Kohn-Sham equation where the output density  $n^{\text{out}}(\mathbf{r})$  is equal to the input density  $n^{\text{in}}(\mathbf{r})$  can be generalized to the following fixed point equation:

$$\mathbf{F}(\mathbf{x}) = \mathbf{x}, \quad (1)$$

$\mathbf{x}$  denotes a vector in many dimensions, e.g. the density is expanded in the dimensions of a set of plane waves. This becomes a minimization problem for the norm of the residual  $\|\mathbf{R}(\mathbf{x})\|$ :

$$\mathbf{R}(\mathbf{x}) \equiv \mathbf{F}(\mathbf{x}) - \mathbf{x}. \quad (2)$$

The simplest method for seeking the solution of Eq. (1) is the fixed point iteration as follows:

$$\mathbf{x}_{m+1} = \mathbf{F}(\mathbf{x}_m). \quad (3)$$

If one is in a region where  $\mathbf{F}$  is a linear function of  $\mathbf{x}$  and  $\mathbf{x}^*$  is the solution of Eq' (1), we have

$$\mathbf{x}_{m+1} - \mathbf{x}^* = \left( \frac{\delta \mathbf{F}}{\delta \mathbf{x}} \right)^m (\mathbf{x}_1 - \mathbf{x}^*).$$

Therefore, a necessary condition that guarantees the convergence of the fixed point iteration is

$$\sigma \left( \frac{\delta \mathbf{F}}{\delta \mathbf{x}} \right) < 1,$$

where  $\sigma(A)$  is the spectral radius of the operator (or matrix)  $A$ . However, in the Kohn-Sham density functional theory, the above condition is generally not satisfied [5].

However, the simple mixing can be made to convergence as long as  $\sigma \left( \frac{\delta \mathbf{F}}{\delta \mathbf{x}} \right)$  is bounded. The simple mixing scheme takes the form:

$$\mathbf{x}_{m+1} = \mathbf{x}_m + P \mathbf{R}(\mathbf{x}_m), \quad (4)$$

where  $P$  is the matrix whose size is equal to the number of basis functions. We define the Jacobian matrix:

$$J \equiv -\frac{\delta \mathbf{R}}{\delta \mathbf{x}} = I - \frac{\delta \mathbf{F}}{\delta \mathbf{x}}, \quad (5)$$

and denote its value at  $\mathbf{x}^*$  by  $J_*$ . When  $\mathbf{x}_m$  are sufficiently close to  $\mathbf{x}^*$ , the error propagation of simple mixing Eq. (4) is given by:

$$\mathbf{x}_{m+1} - \mathbf{x}^* \approx (I - PJ_*) (\mathbf{x}_m - \mathbf{x}^*). \quad (6)$$

In some literatures [3, 5, 15],  $P$  is  $\alpha I$  with  $\alpha$  the scalar parameter. Then it follows from Eq. (6) that simple mixing will lead to convergence if:

$$\sigma(I - \alpha J_*) < 1. \quad (7)$$

If  $\lambda(J_*)$  is an eigenvalue of  $J_*$ , then the inequality Eq. (7) indicates that:

$$\|1 - \alpha \lambda(J_*)\| < 1. \quad (8)$$

Note that  $\lambda(J_*) > 0$  is referred to as the stability condition of the material in [19]. And it holds in most cases according to the analysis given in [5]. Consequently, Eq. (8) implies that:

$$0 < \alpha < \frac{2}{\lambda(J_*)}. \quad (9)$$

When  $\lambda(J_*)$  is bounded, it is always possible to find a parameter  $\alpha$  to ensure the convergence of the simple mixing scheme. Nevertheless,  $\lambda(J_*)$  can become very large in practice, especially in the case of metallic systems with large dimensions, which makes the convergence of the simple mixing extremely slow. Therefore it is desirable to construct effective preconditioning matrix  $P$  in Eq. (4) to speed up the convergence.

Here we want to explicitly show that in the context of the charge mixing, the Jacobian matrix  $J$  is just the charge dielectric response function, which describes the charge response to an external charge perturbation. Replacing the  $\mathbf{x}_m$  in Eq. (4) with charge density  $\mathbf{n}_m$ , we have:

$$\mathbf{n}_{m+1} = \mathbf{n}_m + P \cdot \mathbf{R}(\mathbf{n}_m) \quad (10)$$

For  $\mathbf{R}(\mathbf{n}_m)$ , we could expand it to the linear order as:

$$\mathbf{R}(\mathbf{n}) = \mathbf{R}(\mathbf{n}_m) - J \cdot (\mathbf{n} - \mathbf{n}_m) \quad (11)$$

The  $J$  in the above equation is just the Jacobian matrix defined earlier in Eq. (5). We always want to achieve the self consistency in the next step, such that  $\mathbf{R}(\mathbf{n}_{m+1}) \approx 0$ . Plugging this into Eq. (11), we have:

$$\mathbf{n}_{m+1} = \mathbf{n}_m + J^{-1} \cdot \mathbf{R}(\mathbf{n}_m) \quad (12)$$

Comparing this equation with Eq. (10), we see that  $P = J^{-1}$ . The problem then becomes finding a good approximation of the Jacobian matrix  $J$ . To prove that  $J$  has the physical meaning of charge dielectric function, we follow Vanderbilt and Louie's procedure [13] to show that:

$$\mathbf{V}_{m+1} \approx \mathbf{V}_m + U \cdot (\mathbf{n}_{m+1} - \mathbf{n}_m) \quad (13)$$

where the matrix  $U$  describe the change in the potential due to a change in the charge density. As a result, the output charge density is given by:

$$\mathbf{n}_{m+1}^{\text{out}} \approx \mathbf{n}_m^{\text{out}} + \chi \cdot (\mathbf{V}_{m+1} - \mathbf{V}_m) \quad (14)$$

where  $\chi$  is just the electric susceptibility matrix, describing the change in the output charge density due to a change in the potential. Combining Eqs. (10), (11), (13) and (14), we arrive at:

$$J = I - \chi \cdot U \quad (15)$$

$J$  is often called as the dielectric matrix. According to Vanderbilt and Louie [13],  $J^{-1}$  is the *charge* dielectric response function which describes the fluctuation in the total charge due to a perturbation from external charge. Reversing the order of Eqs. (13) and (14) and adopting the potential mixing, we can also obtain a dielectric response function  $(I - U \cdot \chi)^{-1}$  which describes the potential response to an external potential perturbation. Note that the order of the matrix product matters and generally the *charge* dielectric response function and *potential* dielectric response function are different but closely related.

Also note that this derivation is independent of the basis set, which could either be a plane-wave basis set or atomic-orbital basis set. As mentioned before, a good preconditioning scheme is to mimic the charge dielectric response in the charge mixing at a reasonable computational cost. A detailed discussion of the Kerker preconditioning model will be presented in the next section.

## B. Pulay's method

Instead of using vector  $\mathbf{x}_m$  only from last step in (4), we could minimize the norm of the residual  $\|\mathbf{R}(\mathbf{x})\|$  by using the best possible combination of the  $\mathbf{x}_m$  from all previous steps. This is the idea behind the technique called Direct Inversion in the Iterative Subspace (DIIS). The technique is originally developed by Pulay for accelerating the Hartree-Fock calculation [9]. Hence it is often referred to as Pulay mixing in the condensed matter physics community.

In Pulay's original work [9], the optimal approximation to the next vector is presented as:

$$\mathbf{x}_{m+1} = \sum_{i=0}^{l-1} a_{m-i} \mathbf{x}_{m-i}, \quad (16)$$

where  $l = \min\{m, L\}$  with  $m > 0$  and  $L$  being the maximal dimension of the subspace. We choose the coefficients  $a_{m-i}$  in Eq. (16) through solving the constraint optimization problem:

$$\begin{cases} \min_{\{a_{m-i}\}} \left\| \mathbf{R} \left( \sum_{i=0}^{l-1} a_{m-i} \mathbf{x}_{m-i} \right) \right\|^2 \\ \text{s.t. } \sum_{i=0}^{l-1} a_{m-i} = 1, \end{cases} \quad (17)$$

where  $\|\cdot\|$  is some norm derived from the inner product  $\langle \cdot \rangle$ . To improve the numerical stability [4], we construct the next input vector as

$$\mathbf{x}_{m+1} = \mathbf{x}_m - \sum_{i=1}^{l-1} b_{m-i} \delta \mathbf{x}_{m-i}, \quad (18)$$

where  $\delta \mathbf{x}_{m-i} = \mathbf{x}_{m-i+1} - \mathbf{x}_{m-i}$ . Then the coefficients  $b_{m-i}$  are determined by solving the unconstraint optimization problem:

$$\min_{\{b_{m-i}\}} \left\| \mathbf{R} \left( \mathbf{x}_m - \sum_{i=1}^{l-1} b_{m-i} \delta \mathbf{x}_{m-i} \right) \right\|^2 \quad (19)$$

When the vectors  $\mathbf{x}_{m-i}$  are all sufficiently close to the solution of Eq. (1), the linearity of the residual near the solution leads to:

$$\begin{aligned} & \frac{1}{2} \frac{\partial}{\partial b_{m-i}} \langle \mathbf{R}(\mathbf{x}_{m+1}) | \mathbf{R}(\mathbf{x}_{m+1}) \rangle \\ &= - \langle \delta \mathbf{R}_{m-i} | \mathbf{R}(\mathbf{x}_m) \rangle + \sum_{j=1}^{l-1} b_{m-j} \langle \delta \mathbf{R}_{m-i} | \delta \mathbf{R}_{m-j} \rangle. \end{aligned} \quad (20)$$

Let

$$A_{ij} = \langle \delta \mathbf{R}_{m-i} | \delta \mathbf{R}_{m-j} \rangle, \quad i, j = 1, 2, \dots, l-1, \quad (21)$$

and the solution of Eq. (19) can be presented as:

$$\mathbf{b}_{m-i} = \sum_{j=1}^{l-1} (A^{-1})_{ij} \langle \delta \mathbf{R}_{m-j} \mid \mathbf{R}(\mathbf{x}_m) \rangle. \quad (22)$$

Inserting Eq. (18) into Eq. (4), we obtain:

$$\mathbf{x}_{m+1} = \mathbf{x}_m + P \mathbf{R}(\mathbf{x}_m) - \sum_{j=1}^{l-1} \left[ \sum_{i=1}^{l-1} (A^{-1})_{ij} (\delta \mathbf{x}_{m-i} + P \delta \mathbf{R}(\mathbf{x}_{m-i})) \right] \langle \delta \mathbf{R}_{m-j} \mid \mathbf{R}(\mathbf{x}_m) \rangle \quad (23)$$

An alternative way to derive Pulay's method is taking it as the special case of the Broyden's method [20]. In the Broyden's second method, a sequence of low-rank modifications are made to some initial guess of the inverse of the Jacobian matrix Eq. (5) near the solution of Eq. (1). The recursive formula [6, 21] can be derived from the following constrained optimization problem:

$$\begin{cases} \min_H \frac{1}{2} \|H - H_{m-1}\|_F^2 \\ \text{s.t. } HY_m = -S_m, \end{cases} \quad (24)$$

where  $H_{m-1}$  is the approximation to the inverse Jacobian in the  $m$ th Broyden update,  $S_m$  and  $Y_m$  are respectively defined as:

$$\begin{aligned} S_m &= (\delta \mathbf{x}_m, \delta \mathbf{x}_{m-1}, \dots, \delta \mathbf{x}_{m-l+1}), \\ Y_m &= (\delta \mathbf{R}(\mathbf{x}_m), \delta \mathbf{R}(\mathbf{x}_{m-1}), \dots, \delta \mathbf{R}(\mathbf{x}_{m-l+1})). \end{aligned} \quad (25)$$

It can be shown that the solution to Eq. (24) is (proved in the appendix):

$$H_m = H_{m-1} - (S_m + H_{m-1} Y_m) (Y_m^T Y_m)^{-1} Y_m^T. \quad (26)$$

We arrive at Pulay's method by fixing  $H_{m-1}$  in Eq. (26) to the initial guess  $H_1$  of the inverse Jacobian: Eq. (26) to the initial guess  $H_1$  of the inverse Jacobian

$$H_m = H_1 - (S_{m-1} + H_1 Y_{m-1}) (Y_{m-1}^T Y_{m-1})^{-1} Y_{m-1}^T. \quad (27)$$

Then one can follow the quasi Newton approach to generate the next vector:

$$\mathbf{x}_{m+1} = \mathbf{x}_m + H_m \mathbf{R}(\mathbf{x}_m) \quad (28)$$

$$= \mathbf{x}_m + H_1 \mathbf{R}(\mathbf{x}_m) - (S_{m-1} + H_1 Y_{m-1}) (Y_{m-1}^T Y_{m-1})^{-1} Y_{m-1}^T \mathbf{R}(\mathbf{x}_m). \quad (29)$$

Note that it is natural to take the  $l_2$  norm in Eq. (17) or (19) with plane wave basis. Therefore it is obvious that Eq. (29) is the matrix representation of Eq. (23).

We should comment that the construction of  $H_1$  in Eq. (29) is crucial for accelerating the convergence since it can work as a preconditioner for the simple mixing Eq. (4). It is implied by Eq. (7) that preconditioning will be probably effective if  $H_1$  is a good guess of the inverse Jacobian near the solution of Eq. (1).

### III. PRECONDITIONING MODEL

#### A. Thomas-Fermi screening model

The Thomas-Fermi screening model is the foundation for the Kerker preconditioner, and many other preconditioning scheme as well. In this section, the derivation of the Thomas-Fermi screening model, i.e. the dielectric response function of the homogeneous electron gas, will first be given. In what follows, the implications of this screening model on the convergence issues and Kerker preconditioning model will then be discussed in detail.

Consider an external defect charge distribution (or some small perturbation in the charge density) being introduced into a homogeneous electron gas. The external potential then solely arises from the external charge and satisfies Poisson's equation:

$$-\nabla^2 V_{ext} = 4\pi n_{ext}(\mathbf{r}) \quad (30)$$

The external charge induces a cloud of screening electrons, resulting in a redistribution of the total potential and charge density. Similarly, we have:

$$-\nabla^2 V_{tot} = 4\pi n_{tot}(\mathbf{r}) \quad (31)$$

The difference between the total charge density and external charge density gives the induced charge density  $n_{ind}$ . One could assume that  $V_{tot}$  and  $V_{ext}$  are linearly related through the relation [22]:

$$V_{ext}(\mathbf{r}) = \int d\mathbf{r}' \varepsilon(\mathbf{r}, \mathbf{r}') V_{tot}(\mathbf{r}') \quad (32)$$

In the homogeneous electron gas, the dielectric matrix  $\varepsilon$  would only depends on the distance between the  $\mathbf{r}$  and  $\mathbf{r}'$ . Thus Eq. (32) becomes:

$$V_{ext}(\mathbf{r}) = \int d\mathbf{r}' \varepsilon(\mathbf{r} - \mathbf{r}') V_{tot}(\mathbf{r}') \quad (33)$$

Under the Fourier transform, we have the following relation for their Fourier components:

$$V_{ext}(\mathbf{q}) = \varepsilon(\mathbf{q}) V_{tot}(\mathbf{q}) \quad (34)$$

If the perturbation is weak and slow-varying in space (which is probably a good approximation near the self consistency), the induced charge density  $n_{ind}$  and the total potential  $V_{tot}$  are linearly linked by:

$$n_{ind}(\mathbf{q}) = \chi(\mathbf{q})V_{tot}(\mathbf{q}) \quad (35)$$

We note that this relation shares the same spirit with Eq. (14). The Fourier transforms of the Poisson Eqs. (30) and (31) are:

$$\mathbf{q}^2 V_{ext}(\mathbf{q}) = 4\pi n_{ext}(\mathbf{q}) \quad (36)$$

$$\mathbf{q}^2 V_{tot}(\mathbf{q}) = 4\pi n_{tot}(\mathbf{q}) \quad (37)$$

Combining Eqs. (34), (35), (36) and (37), we have the relation between  $\varepsilon$  and  $\chi$ :

$$\varepsilon(\mathbf{q}) = 1 - 4\pi \frac{\chi(\mathbf{q})}{\mathbf{q}^2} \quad (38)$$

Note that this is consistent with the general form given in Eq. (15). The dielectric matrix  $\varepsilon$  (or  $J$  in the context of previous section) is diagonalized due to the homogeneity of the system and can be seen as a function of  $\mathbf{q}$ . Now we focus on the calculation of the quantity  $\chi(\mathbf{q})$ . The induced charge density is the difference between systems with and without the external potential:

$$n_{ind}(\mathbf{r}) = -e[N(\mu + eV(\mathbf{r})) - N(\mu)] \quad (39)$$

where the electron number density  $N$  as a function of chemical potential  $\mu$  is given by the Fermi-Dirac distribution and dispersion relation of the free electron gas:

$$N(\mu) = \int \frac{d\mathbf{k}}{4\pi^3} \frac{1}{\exp[\beta(\frac{\hbar^2 \mathbf{k}^2}{2m_e} - \mu)] + 1} \quad (40)$$

Based on the assumption that the external potential is weak and slow-varying in space, we could expand Eq. (39) near the electron chemical potential  $\mu$  (or the Fermi energy  $\varepsilon_F$ ) to the first order as:

$$n_{ind}(\mathbf{r}) = -e^2 \frac{\delta N}{\delta \mu} V(\mathbf{r}) \quad (41)$$

where the quantity  $\frac{\delta N}{\delta \mu}$  is proportional to the number of states in the vicinity of the electronic chemical potential or Fermi level. Comparing Eqs. (41) and (35), we have:

$$\chi(\mathbf{q}) = -e^2 \frac{\delta N}{\delta \mu} \quad (42)$$

Thus, Eq. (38) now becomes:

$$\varepsilon(\mathbf{q}) = 1 + \frac{k_{TF}^2}{\mathbf{q}^2} \quad (43)$$

This is the dielectric function of the Thomas-Fermi screening model [42]. The Thomas-Fermi vector  $k_{TF}$  is defined through:

$$k_{TF}^2 = 4\pi e^2 \frac{\delta N}{\delta \mu} \quad (44)$$

Since the preconditioner is the inverse of the dielectric function, we now have a preconditioner that is based on this screening model:

$$H_1^{TF}(\mathbf{q}) = \frac{\mathbf{q}^2}{\mathbf{q}^2 + k_{TF}^2} \quad (45)$$

This is just the form of the Kerker preconditioner [3, 11, 15]. We would like to remark few things regarding the Thomas-Fermi screening model with its implication to SCF loop and Kerker preconditioner:

- a)** According to Eq. (43), at small  $\mathbf{q}$  or long wavelength, the dielectric function diverges quadratically. Assume a metallic system contains small  $\mathbf{q}$ 's. Then in the SCF loop, changes in the charge density will cause large changes in the potential (or more precisely, the Hartree potential) at long range. This, in turn, results in large and long-range changes in the output charge density, known as the "charge sloshing", thus causes the convergence hard to achieve. Such convergence issue is more prominent in the long-z metallic slab systems in which one dimension of the cell is much larger than the rest two. Therefore we focus our numerical tests on the slab systems.
- b)** The contribution from the exchange-correlation potential is neglected in the derivation. The exchange-correlation potential value, under the local density approximation (LDA) or generalized gradient approximation (GGA), depends on the local charge density (plus its derivatives in the case of GGA). In the long wavelength limit, this type of local potential is much smaller in magnitude compared to the Coulomb potential, which behaves as  $1/\mathbf{q}^2$  divergence at small  $\mathbf{q}$ . In this sense, the Thomas-Fermi screening as well as the Kerker preconditioning model are getting the correct behavior at the long wavelength limit but losing some details of responses at large  $\mathbf{q}$ . We also note the Thomas-Fermi screening model also gets the large- $\mathbf{q}$  limit right, where the dielectric response goes to 1. Based on our numerical results, we believe predicting a (qualitatively) correct behavior of the preconditioner at small  $\mathbf{q}$  is the key part for speed up the convergence.

c) Even though the dielectric function in Eq. (43) is mounted on the homogeneous electron gas, it still manifests a important feature of the electron screening in the metallic system. As mentioned above,  $\frac{\delta N}{\delta \mu}$  has the physical meaning of the number of the states in the vicinity of (below and above) the Fermi level. We can interpret this as: the electrons near the Fermi level are actively involved in screening since they can adjust themselves to higher unoccupied states to accommodate the change in the potential. On the other hand, deeper electrons are limited by the high excitation energy or Pauli exclusion principle. This observation is somehow independent of the band structures of the system.

d) Following the above point, we further estimate the relation between the electron density and the parameter  $k_{TF}$  under the assumption of homogeneous electron gas. Since  $\frac{\delta N}{\delta \mu}$  can be approximated by the number of states at the Fermi level, we can write  $k_{TF}$  as:

$$k_{TF}^2 \approx 4\pi e^2 N(\varepsilon_F) = \frac{4(3\pi^2 n_0)^{1/3}}{a_B \pi} \quad (46)$$

where  $a_B$  is the Bohr radius and  $n_0$  is the total free electron density in the system:

$$a_B = \hbar^2/(me^2) \approx 0.53 \text{ \AA} \quad (47)$$

Plugging in numbers, we have the following relation:

$$k_{TF} \approx 2\left(\frac{n_0}{a_B^3}\right)^{1/6} \quad (48)$$

In a typical metal,  $n_0 \approx 10^{23} \text{ cm}^{-3}$ . Therefore,  $k_{TF} \approx 1 \sim 2 \text{ \AA}^{-1}$ . This is also the default value range used for most Kerker preconditioner in the calculations. As shown later in our examples, Eq. (48) could offer us guide to parameterized the  $k_{TF}$  and facilitates the convergence of the metal-insulator hybrid systems and insulating systems with metal-like defect states.

## B. Resta screening model

The Thomas-Fermi screening model is more appropriate in describing the screening effect in the metallic system. Resta revised the boundary condition of the previous Poisson equation Eq. (31) and derived the screening model for semiconductors and insulators [23]. Rather than being complete screened at the long range in the metallic system, the potential is only

partially screened beyond some screening length in the insulators. This is characterized by the static dielectric constant  $\varepsilon(0)$ :

$$V(\mathbf{r}) = -\frac{Z}{\varepsilon(0)r}, \quad r \geq R_s \quad (49)$$

Where  $R_s$  is the screening length which is generally on the order of the lattice constants. According to Resta, the relation between the screening length and the static dielectric constant is given by:

$$\varepsilon(0) = \frac{\sinh(q_0 R_s)}{q_0 R_s} \quad (50)$$

where  $q_0$  is a constant related to the valence electron Fermi momentum  $k_F$ :

$$q_0 = (4k_F/\pi)^{1/2} \quad (51)$$

with  $k_F$  related to the average valence electron density  $n_0$  by:

$$k_F = (3\pi n_0)^{1/3} \quad (52)$$

Under the atomic unit,  $q_0$  is in the unit of 1 over distance. The dielectric function can be written as follow:

$$\varepsilon(\mathbf{q}) = \frac{q_0^2 + \mathbf{q}^2}{\frac{q_0^2 \sin(|\mathbf{q}| R_s)}{\varepsilon(0) |\mathbf{q}| R_s} + \mathbf{q}^2} \quad (53)$$

The three material parameters  $q_0$ ,  $R_s$  and  $\varepsilon(0)$  in the above equation are related by Eq. (50) thus only two are needed for the input. The static dielectric constant  $\varepsilon(0)$  and Fermi momentum related quantity  $q_0$  can be extracted from the experimental data. In Resta's original paper, he offered the input parameters for Diamond, Silicon and Germanium in his original paper. He further showed that the Resta's dielectric functions for these materials are in close agreement with others derived from Penn-model results of Srinivasan [24, 25] and RPA calculations of Walter and Cohen [26]. However, the dielectric function he proposed is much simpler in the expression compared with others. Later on, Shajan and Mahadevan [27] used Resta's model to calculate the dielectric function of many binary semiconductors, such as GaAs, InP, ZnS, etc. Their results are found to be in excellent agreement with those calculated by the empirical pseudopotential method [28].

Here, we proposed the Resta's preconditioner which is based on Resta's model has the following form:

$$H_1^{Res}(\mathbf{q}) = \frac{\frac{q_0^2 \sin(|\mathbf{q}| R_s)}{\varepsilon(0) |\mathbf{q}| R_s} + \mathbf{q}^2}{q_0^2 + \mathbf{q}^2} \quad (54)$$

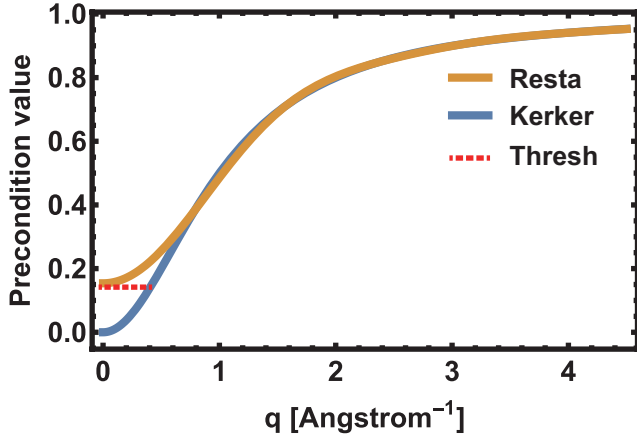


FIG. 1: (color online) The preconditioning models as a function of reciprocal vector  $\mathbf{q}$ . A threshold parameter can be added to the Kerker preconditioner to simulate the small  $\mathbf{q}$  behavior of the insulating systems.

It is instructive to compare this preconditioner with Kerker preconditioner. The two preconditioners are plotted as the function of  $\mathbf{q}$  in Fig. 1. For Kerker preconditioner, the  $k_{TF}$  is chosen to be 1, in the unit of  $\text{\AA}^{-1}$ . For the Resta preconditioner, the static dielectric constant is chosen to be 6.5. For many semiconductors and insulators, this value falls into the range of  $5 \sim 15$ . The  $q_0$  is chosen to be  $1 \text{\AA}^{-1}$  and the screening length is  $4 \text{\AA}$ , accordingly. These values are about the typical inputs for all binary semiconductors studied in [27]. From Fig.1, it is helpful to point out the following points:

- a)** At some  $\mathbf{q}$  values slightly below 1, the two curves start to merge. At relatively large  $\mathbf{q}$ , they all converge to 1. This means the dielectric responses of metallic and insulating systems are the same at the short wavelength limit. This behavior, reflected in the preconditioners, leads to a simple mixing scheme for the large  $\mathbf{q}$  components.
- b)** The essential difference between the Kerker preconditioner and Resta preconditioner (and screening model as well) happens at small  $\mathbf{q}$  limit. For the Kerker preconditioner, as we have discussed in the previous section, it goes to zero quadratically. While for the Resta preconditioner, it goes to a finite value at  $\mathbf{q}$  equals zero and this value is just  $1/\varepsilon(0)$ . This represents the incomplete screening in the insulating systems due to a lack of conducting electrons. We also note if a nominal insulating system contains metal-like defect states (in other words there is an incompletely filled defect states), Resta preconditioner does not offer too much help in speeding up the convergence.

c) In practical, if one does not want to switch between the two preconditioning models when calculating different systems, a threshold can be added to the Kerker preconditioner to mimic the behavior of the Resta preconditioner at the small  $\mathbf{q}$ 's, as shown by the dashed line in the Fig. 1. Now the revised Kerker preconditioner has the form:

$$H_1^{TF'}(\mathbf{q}) = \max(a_0, \frac{\mathbf{q}^2}{\mathbf{q}^2 + k_{TF}^2}) \quad (55)$$

In the revised Kerker preconditioner, it will move part of the curve that is below  $a_0$  to  $a_0$ . This action restores the behavior of the screening effect in the insulating systems. In the code, the threshold parameter  $a_0$  is set with a linear mixing parameter  $\alpha$  multiplying the preconditioner.

$$H_1^{TF''}(\mathbf{q}) = \max(a_0, \alpha \frac{\mathbf{q}^2}{\mathbf{q}^2 + k_{TF}^2}) \quad (56)$$

Accordingly, the optimal  $a_0$  should be equal to  $\alpha/\varepsilon(0)$ . This modification extended the applicability of the Kerker preconditioner.

#### IV. NUMERICAL EXAMPLES

We have performed the convergence tests on various systems using the in-house code CESSP [29, 30] under the infrastructure of JASMIN [31]. The exchange and correlation energy is described by the generalized gradient approximation proposed by Perdew, Burke, and Ernzerhof [32]. Electron-ion interactions are treated with projector augmented wave potentials [33]. The first 5 steps of the iteration take the Blocked Davison scheme where no charge mixing takes place [34]. The following steps take the RMM-DIIS scheme [3]. The mixing parameter  $\alpha$  is set to 0.4 in all calculations with different preconditioners. The convergence criterion for self-consistent field loop is  $1 \times 10^{-6}$  eV, which is a good enough criterion for practical slab system calculations. When constructing the slab models, we always include at least 20 Å of vacuum layer, which is used to exclude the spurious interaction between surfaces under the periodic boundary condition.

##### A. Au slab: the metallic system

The first system is the {111} Au slabs. We have constructed three Au slab systems with 14, 33 and 54 layer of Au {111} planes, corresponding to a cell parameter of 5, 11 and 15

TABLE I: The number of convergence steps in the Au slab systems.

number of Au layers	total slab thickness [nm]	number of steps
14	5	27
36	11	32
54	15	31

nm along the direction normal to Au  $\{111\}$  surface, respectively. A  $12 \times 12 \times 1$  k-point grid is used to sample the Brillouin zone. The cutoff energy is chosen to be 350 eV. Here, the Kerker preconditioner with no threshold parameter  $a_0$  (referred as "original Kerker preconditioner") has been used to speed up the convergence. The  $k_{TF}$  has been set to 1 in the unit of  $\text{\AA}^{-1}$ . The number of iterations to reach the convergence is listed in Table I.

The Kerker preconditioner works fairly well in converging of long-z Au slab systems. In addition, the number of steps is weakly dependent on the size of the system, which is also an indication that the charge sloshing has been suppressed. Even though Au is not regarded as a "free-electron" like metal, the Kerker preconditioner still speeds up the convergence. As we have stated in the previous section, the charge sloshing phenomenon is a reflection of the quadratical divergence of the dielectric function at  $\mathbf{q} \rightarrow 0$  limit. The Thomas-Fermi model and the Kerker preconditioner are getting the small  $\mathbf{q}$  behavior right, even though the free electron gas model is not a good approximation for Au as well as many realistic metallic systems.

### B. $\text{MoS}_2$ : the layered insulating system

Secondly, we have studied the convergence of the layered insulating system:  $\text{MoS}_2$ . Two slab systems with 10 and 20 layers of  $\text{MoS}_2$ , corresponding to a cell parameter of 8 nm and 16 nm, have been constructed. The  $\text{MoS}_2$  layers have been stacked in the same fashion as those in the bulk  $\text{MoS}_2$ . A  $6 \times 6 \times 1$  k-point grid has been used to sample the Brillouin zone. The cutoff energy is 450 eV. Both Kerker and Resta preconditioners have been tested on the  $\text{MoS}_2$  slab systems.

For the Resta preconditioner, we need the static dielectric constant and screening length as input parameters. We have found the reported value of the average static elastic constant

of  $\text{MoS}_2$  varying in the past literature [35–38]. It is also found that the static elastic constant depends on the number of  $\text{MoS}_2$  layers. However, the value of it all falls into the range of  $5 \sim 15$ . Thus we have used three static dielectric constants 5, 10 and 15, in the Resta preconditioner. The screening length  $R_s$  has been set to 3.5 which is close to the lattice constants. The  $q_0$  in the Resta model is then calculated by Eq. (50).

For the Kerker preconditioner, we adopt both the original preconditioner and the revised Kerker preconditioner. In both cases, the Thomas-Fermi vector  $k_{TF}$  has been set to  $1 \text{ \AA}^{-1}$ . For the revised Kerker preconditioner, we have chosen the threshold parameters  $a_0$  according to the dielectric constants in the Resta model. The threshold parameters are  $1/5, 1/10$  and  $1/15$  accordingly.

TABLE II: The number of convergence steps in the  $\text{MoS}_2$  slab systems.

Precondition model	10 layer $\text{MoS}_2$	20 layer $\text{MoS}_2$
Kerker	38	52
Resta( $\varepsilon(0) = 5$ )	25	26
Resta( $\varepsilon(0) = 10$ )	30	31
Resta( $\varepsilon(0) = 15$ )	32	32
Revised Kerker ( $a_0 = 0.4/5$ )	27	27
Revised Kerker ( $a_0 = 0.4/10$ )	28	32
Revised Kerker ( $a_0 = 0.4/15$ )	28	32

We further plot the convergence of energies between the original Kerker preconditioner, the revised Kerker preconditioner and the Resta preconditioner in Fig. 2. For the revised Kerker preconditioner and the Resta preconditioner, we choose the results from those with dielectric constant of 10. The first 5 steps are blocked Davison scheme thus we plot the energy versus steps from the 6th step.

From Table II and Fig. 2, it is clear that the Resta model and the revised Kerker model converge the energies faster than the original Kerker model, since the  $\text{MoS}_2$  slab systems are insulator. Both the Resta model and the revised Kerker model give a correct behavior of the screening effect at small  $\mathbf{q}$ 's. In addition, using 5, 10 or 15 for the static dielectric constant gives similar results. Therefore, the convergence speed is not that sensitive to the value of static dielectric constant and corresponding parameters.

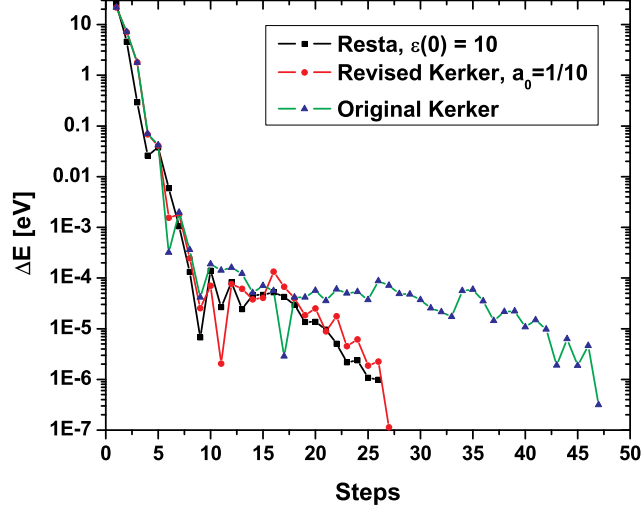


FIG. 2: (color online) The convergence of energies in 20 layer MoS<sub>2</sub> correponding to different preconditioning models.

### C. Si slab: the insulating system containing defect states

Even though Resta preconditioner seems to be more appropriate for the insulating systems based on the previous example, we want to further show that this is not the case for the "nominal" insulating systems but containing defect states cross the Fermi level. A 96 layer Si slab has been constructed with the {111} orientation with a cell parameter of 175 Å in the  $z$  direction. Both the top and bottom Si surfaces have one dangling bond due to the creation of the surface. A  $6 \times 6 \times 1$  k-point grid has been used to sample the Brillouin zone. The cutoff energy is 320 eV. The dielectric constant of bulk Si is about 12. The screening length  $R_s$  is 4.2 Å and the  $q_0$  is chosen as 1.1 Å<sup>-1</sup>, in accord with Resta's parameterizations [23]. As in the case of MoS<sub>2</sub>, we compare the convergence speed between the three preconditioning models. The calculated results are shown in Table III.

TABLE III: The number of convergence steps in the Si slab system.

Preconditioning model	number of steps
Kerker	40
Revised Kerker ( $a_0 = 0.4/12$ )	52
Resta	47

In this case, the original Kerker preconditioner offers the fastest convergence compared

with the rest two, which goes against with the conclusion from the previous section. Why is the convergence behavior of the Si slab different from the  $\text{MoS}_2$  slab? After careful inspection, we have found that it is the surface states of the Si slab that deviate the system from a "perfect" insulating system. The density of states (DOS) of the Si slab and the

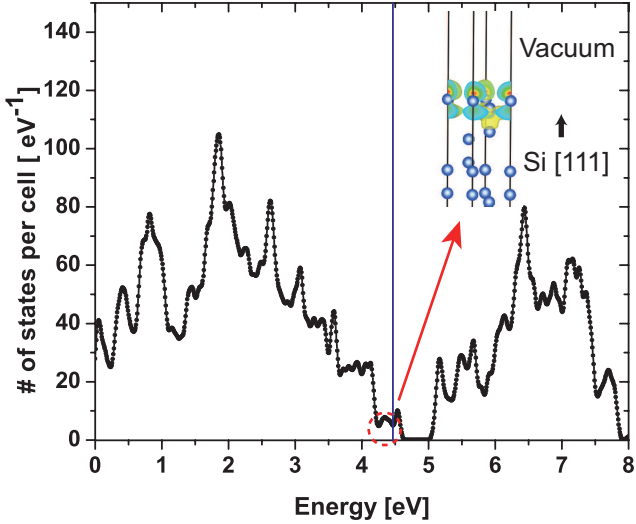


FIG. 3: (color online) The density of states (DOS) of the 96-atom Si slab. The vertical blue line indicates the Fermi level. The states right below the Fermi level are the surface states, as shown by the partial charge density plot. The bottom surface is identical to the top surface thus only one is shown.

corresponding partial charge density distribution of these states have been plotted in Fig. 3. From the figure, we can see that the creation of the surface introduces defect states right at the Fermi level. The presence of these states drives the system away from a "perfect" insulating system, since there is now allowable states right above the Fermi level. This essential difference makes the preconditioning models suited for insulator much less effective in the Si slab system. In our previous case, since the  $\text{MoS}_2$  is a natural layered material, it will not introduce surface states through creating the slab from the bulk.

To further prove our idea, we passivate the Si surfaces by the hydrogen atoms. Now the system contains 96 layer of Si with 2 extra layer of H covering the top and bottom Si surfaces in the same unit cell. The calculation parameters are kept same. The convergence speed versus different preconditioning models is shown in the Table IV. Now the trend is consistent with what we have seen in the case of  $\text{MoS}_2$ , in which the revised Kerker (29 steps) and Resta models (30 steps) works better than the original Kerker model (46 steps). Indeed

TABLE IV: The number of convergence steps in the H passivated Si slab system.

Preconditioning model	number of steps
Kerker	46
Revised Kerker ( $a_0 = 1/12$ )	29
Resta	30

the extra H layers have passivated the dangling bonds on the Si surfaces and removed the surface states. We further plot the DOS of the H passivated Si slab in Fig. 4. In sum, the

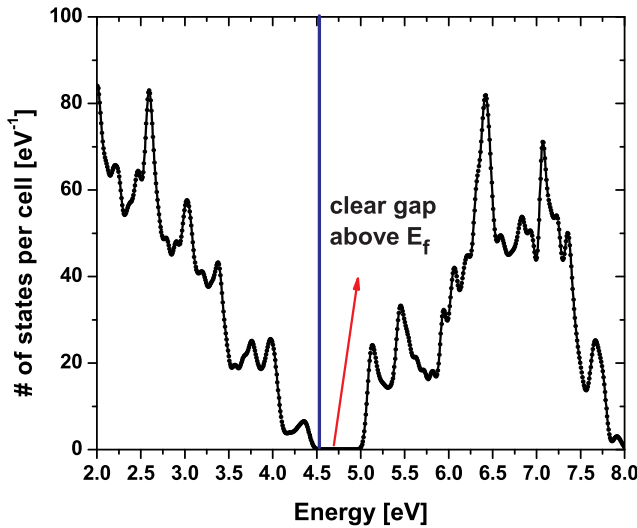


FIG. 4: (color online) The density of states (DOS) of the Si slab with H passivation (96 layer of Si with 2 H passivation layer on the top and bottom Si surfaces). The vertical blue line indicates the Fermi level. The added H layers remove the surface states. A clear band gap now occurs right above the Fermi level.

revised Kerker preconditioner and Resta preconditioner are better suited for the "prefect" insulating systems. However, introducing metal-like states crossing the Fermi level from defects would render these preconditioning models much less effective.

#### D. Au-MoS<sub>2</sub>: the metal-insulator hybrid system

Finally we want to discuss the case of metal-insulator hybrid systems. The example system used in our numerical tests combines multiple layers of {111} Au and multiple layers

of  $\text{MoS}_2$ . The Au layers and  $\text{MoS}_2$  layers are closely welded by a distance of the covalent bond length. Such structural models have been studied using DFT previously to understand the surface, interface and contact properties of Au- $\text{MoS}_2$  epitaxial systems [39–41]. However, for the purpose of evaluating the performance of the preconditioning models in this paper, we have constructed slab systems that are much thicker.

Many Au- $\text{MoS}_2$  slabs with different proportion of Au and  $\text{MoS}_2$  have been created. These slab systems share the same cell parameters and nearly same slab thicknesses and total number of atoms. The total length of the cell is 160 Å with  $\sim 25$  Å vacuum layer and  $\sim 135$  Å Au- $\text{MoS}_2$  slab. The total number of the atoms in the cells is about 65 with slight variation when varying the proportion of the Au and  $\text{MoS}_2$ . A  $6 \times 6 \times 1$  k-point grid is used to sample the Brillouin zone. The cutoff energy is 450 eV. The Au- $\text{MoS}_2$  hybrid system is far away from "perfect" insulator and can no longer be described by the Resta preconditioner. Therefore, we are seeking for the optimized parameterization scheme under the Kerker preconditioning model. As will be shown in the following, we can achieve fast convergence of such highly inhomogeneous metal-insulator hybrid system within the framework of Kerker preconditioning model, even though the corresponding screening model is based on the simple homogeneous electron gas.

There are two parameters in the revised Kerker preconditioner that we can play with,  $a_0$  and  $k_{TF}$ , according to Eqs. (45) and (55). Based on previous discussion,  $a_0$  is related to the static dielectric constant. Consider two limits: if the system is full of Au, then  $a_0$  should be set to 0, which goes back to the original Kerker scheme; If the system is solely  $\text{MoS}_2$ , then  $a_0$  can be set to 1/10, as illustrated in the previous section. These two limits set the upper and lower bound for the hybrid systems. Actually, we could estimate the lower bound one step further: the mixing of the charge density is done in the reciprocal space and the smallest  $\mathbf{q}$  that enters the mixing is  $\frac{2\pi}{L}$ , where  $L$  is the longest dimension of the cell. Therefore, using any  $a_0$  value in the revised Kerker scheme smaller than  $H_1^{TF}(\frac{2\pi}{L})$  from Eq. (45) is equivalent to setting  $a_0$  to 0. In the case of Au- $\text{MoS}_2$ ,  $L$  is 160 Å and the calculated minimal effective  $a_0$  is about  $6 \times 10^{-4}$ . However, finding the optimized  $a_0$  is rather difficult since the hybrid system is a highly inhomogeneous system with different parts having distinct responses to the external electric perturbation. The average static dielectric constant is ill defined than those in the insulating systems. Therefore we perform calculations with various  $a_0$  values between the upper and lower bound (uniform on the log scale). The convergence steps versus

different threshold parameters  $a_0$  in the Au-MoS<sub>2</sub> systems are listed in the Table V.

TABLE V: The convergence speed in Au-MoS<sub>2</sub> hybrid systems versus threshold parameter  $a_0$ .

Au-MoS <sub>2</sub> systems	1E-2 <sup>a</sup>	6E-3	3E-3	2E-3	1E-3	8E-4	1E-4
43 Au + 6 MoS <sub>2</sub>	88	87	47	43	50	47	34
27 Au + 12 MoS <sub>2</sub>	76	66	45	32	34	50	49
16 Au + 16 MoS <sub>2</sub>	75	82	39	30	34	45	43
11 Au + 18 MoS <sub>2</sub>	72	103	32	33	32	38	32
5 Au + 20 MoS <sub>2</sub>	99	47	33	40	32	39	47
3 Au + 21 MoS <sub>2</sub>	93	55	31	32	31	33	37
1 Au + 22 MoS <sub>2</sub>	39	39	28	40	39	39	37

<sup>a</sup> $a_0$  larger than 1E-2 generally results in very bad convergence or even divergence. Thus we do not list those results.

From Table V, we can see that for some well chosen  $a_0$ 's, the convergence steps can be less than 35 steps. Most of the well chosen  $a_0$ 's fall into a region between 3E-3 and 1E-3. However, for the cases of 43 (layer) Au + 6 (layer) MoS<sub>2</sub> and 11 Au + 18 MoS<sub>2</sub>, the  $a_0 = 1E - 4$  (equivalent to original Kerker scheme) gives the fastest convergence. A slightly larger  $a_0$  results in much worse convergence speed: generally more than 70 steps for 6E-3 and 1E-2. On the other hand, smaller  $a_0$  also increases the convergence steps in many cases. However, unlike the case of larger  $a_0$ , smaller  $a_0$  leads to acceptable convergence speed. Generally the number of steps is below 50 and in some cases the original Kerker scheme also gives relatively fast convergence.

Even with the numerical results, it is still hard to summarize a rule of thumb for choosing the optimized  $a_0$ . It seems that there exists a region of optimized  $a_0$ . But being slightly outside this region, especially to a larger value of  $a_0$ , leads to much worse convergence speed. Conservatively speaking, the original Kerker scheme can act as a safe choice: for most hybrid systems, this scheme offers acceptable convergence speed.

There is another way to cope the Kerker preconditioner with the hybrid system. According to the discussion of the Kerker model and Eq. (48),  $k_{TF}$  is related to the number of free electrons in the system. Starting from the system of solely Au, increasing the proportion

of  $\text{MoS}_2$  part means a reduction in the free electrons from Au, and decreasing value of  $k_{TF}$  as a result. For solely Au slab, the value of  $k_{TF}$  is  $1 \text{ \AA}^{-1}$ . Replacing a portion, say  $\alpha$ , of the Au slab with  $\text{MoS}_2$ , reduces the number of free electrons  $n$  to  $(1 - \alpha)n$  since the  $\text{MoS}_2$  makes no contributions to the free electrons. Therefore, the  $k_{TF}$  for the hybrid system can be calculated as  $1 \times (1 - \alpha)^{1/6}$ , according to Eq. (48). For example, in the  $27 \text{ Au} + 12 \text{ MoS}_2$  system, there are total 63 atoms in the system (each  $\text{MoS}_2$  layer contains 3 atoms). Thus the metallic proportion is  $27/63$  and the corresponding  $k_{TF}$  is given by  $(\frac{27}{63})^{(1/6)} \sim 0.87$ . We have checked the convergence speed adopting this parameterization scheme. The results are listed in Table VI together with the results from the optimized  $a_0$  and original Kerker scheme in Table V.

TABLE VI: The convergence speed in Au- $\text{MoS}_2$  hybrid systems versus  $k_{TF}$  and  $a_0$ .

Au- $\text{MoS}_2$ systems	optimized $a_0$	original Kerker	adjusting $k_{TF}$ <sup>a</sup>
43 Au + 6 $\text{MoS}_2$	34	34	33 (0.94)
27 Au + 12 $\text{MoS}_2$	32	49	29 (0.87)
16 Au + 16 $\text{MoS}_2$	30	43	41 (0.8)
11 Au + 18 $\text{MoS}_2$	32	32	31 (0.74)
5 Au + 20 $\text{MoS}_2$	33	47	34 (0.65)
3 Au + 21 $\text{MoS}_2$	31	37	45 (0.6)
1 Au + 22 $\text{MoS}_2$	28	37	22 (0.5)

<sup>a</sup>The estimated values of  $k_{TF}$  are shown in the parenthesis.

According to the results, adjusting  $k_{TF}$  in the above way can offer the fastest convergence in many cases, compared with the results through scanning  $a_0$  between the upper and lower bound. In the  $16 \text{ Au} + 16 \text{ MoS}_2$  system, adjusting  $k_{TF}$  offers slower convergence compared that from the optimized  $a_0$  but slightly fast compared with the original Kerker scheme. Only in the  $3 \text{ Au} + 21 \text{ MoS}_2$  system, adjusting  $k_{TF}$  gives the slowest convergence compared with the rest two. In addition, with small adjustment near the initial  $k_{TF}$ , these two systems can also achieve the fastest convergence. For the  $16 \text{ Au} + 16 \text{ MoS}_2$  system, changing  $k_{TF}$  from initial value 0.8 to 0.85, one can reach the convergence at 31st step. For the  $3 \text{ Au} + 21 \text{ MoS}_2$  system, changing  $k_{TF}$  from 0.6 to either 0.55 and 0.65, the convergence steps become 31 and 32, respectively. We conclude that adjusting  $k_{TF}$  in such way could either give the very fast

convergence or be a good initial guess of further optimizing  $k_{TF}$ . However, adopting this parameterization scheme requires *a priori* knowledge of the system. If we cannot roughly judge which part of the system is metallic or insulating before the calculation, then this scheme is hard to apply.

## V. FURTHER DISCUSSIONS

We would like to address few important points before we reach the final conclusions:

### 1. Preconditioning model and dielectric function

As proved in section of discussing the mixing schemes, the preconditioning model is closely related to the dielectric function of the system. Ideally, the preconditioner would be exactly the inverse of the dielectric function. However, in practical, finding a good preconditioner does not necessarily mean finding the dielectric function as accurately as possible. Because in the context of SCF calculation, the total calculation time to reach the convergence is more of the concern. Spending much time in computing the accurate dielectric function and reaching the convergence in fewer steps might not be as efficient as using a much simpler preconditioner and reaching the convergence in maybe slightly more steps. In this paper, we focus on extending the applicability of the Kerker preconditioning model, which is based on a rather simple dielectric function model, i.e. the Thomas-Fermi screening model.

Meanwhile, we would like to point out that solving for the accurate dielectric response to speed up the convergence is also promising. Many efforts have been devoted in this direction, such as directly solving for the dielectric response of the mixing charge density by Raczkowski *et al.* (in which process the dielectric function is implicitly solved) [12], and reducing the computational cost of directly evaluating the dielectric function using the eigenstates and eigenvalues from the calculation by Anglade *et al.* [18].

### 2. The Thomas-Fermi screening model, generalized Kerker preconditioner, and realistic systems

It is well known that the Thomas-Fermi screening model is built on the homogeneous electron gas system and the Kerker preconditioner is rooted in the Thomas-Fermi screening model. However, based on the numerical examples, we can see that with some simple (but physically meaningful) modifications, the Kerker preconditioner can be generalized to a wide range of materials, including systems that are no way near the free electron gas

system, such as the insulating systems and the metal-insulator hybrid systems. Then what is the merit in the revisement of the generalized Kerker preconditioner? According to our experience, the description of the long-range screening behavior is crucial to reach fast convergence. While in the generalized Kerker scheme, it is possible to capture the essence of this behavior: the original Kerker preconditioner suppress the  $\mathbf{q}^2$  divergence at  $\mathbf{q} \rightarrow 0$  limit in the metallic system; The incomplete screening effect in the insulating systems is captured by the threshold parameter  $a_0$ ; As for the metal-insulator hybrid system, the long-range screening effect is characterized by the effective number of electrons that can participate in the screening and this number is represented in the parameter  $k_{TF}$ . Our numerical examples indeed show the effectiveness of the generalized Kerker preconditioner: converging more than 60 layer slab system (more than 15 nm long in cell parameter) to relatively high accuracy in about 30 steps is significant for practical applications.

### 3. Safe choices and self-adaptive parameterization

Our previous discussions on the revised Kerker scheme and parameterization strategy are mostly based on situations when we have *a priori* knowledge of the systems. But what if we do not? In the first place, we can use some safe-choice settings. The original Kerker preconditioner both seem to be good choices. The original Kerker scheme would work well for the long metallic slab systems and have mediocre convergence performance (no more than 50 steps) on the insulating and hybrid systems.

On the other hand, setting the threshold parameter  $a_0$  will improve the convergence for some insulating systems, but would take risk of worsening the convergence in some metallic systems. To further improve it, we introduce the idea of adaptive parameterization. Outputting the Jacobian matrix during the SCF calculation could give us an idea of the appropriateness of the current preconditioner. Generally speaking, too broad the eigen-spectrum, and based on our experience, especially too small the smallest eigenvalue of the Jacobian matrix, indicate an inappropriate choice of the preconditioner. Then the user can stop the current calculation and set a new  $a_0$ .

We have also made some efforts in trying to realize the self-adaptive parameterization, in which the algorithm updates the preconditioner during the SCF calculation if needed. However, it seems that some global adjustments on the Pulay-Kerker scheme are needed to reach more stable SCF iterations after self-adaptive parameterization has been applied.

## VI. CONCLUSIONS

In sum, we have proposed that the Kerker scheme with physically meaningful modifications can be generalized to improve the convergence of metallic, insulating and metal-insulator hybrid systems. The modifications are taken in two aspects: the threshold parameter  $a_0$  mimics the screening behavior of insulators at long-range limit and helps to better accommodate the insulating systems; The  $k_{TF}$  represents the number of metal-like electrons in the system and can be used to speed up the convergence of metal-insulator hybrid system. Together with our numerical examples, we show that the Kerker preconditioner is effective and efficient for the SCF calculations of inhomogeneous systems.

## APPENDIX

Now we prove Eq. (26) is the solution to the constraint optimization problem Eq. (24). First we prove the following lemma.

**Lemma 1.** *Let  $X \in \mathbb{C}^{m \times n}$ ,  $A \in \mathbb{C}^{n \times p}$ ,  $B \in \mathbb{C}^{m \times p}$ , and assume that  $A$  has full column rank. Denote the Moore-Penrose pseudoinverse of  $A$  by  $A^\dagger$  with  $A = (A^H A)^{-1} A^H$ . If  $XA = B$  is satisfiable, and the matrix  $Z \equiv BA^\dagger$ , then it holds that*

$$\|Z\|_F \leq \|X\|_F \quad (57)$$

*Proof.* Let  $Q \equiv AA^\dagger$ . Then it follows that  $Q^H = Q$  and  $ZQ = Z$ . Thus we have

$$\begin{aligned} (X - Z, Z)_F &\equiv \text{tr} [(X - Z)Z^H] & (58) \\ &= \text{tr} [(X - Z)(ZQ)^H] \\ &= \text{tr} [(X - Z)Q^H Z^H] \\ &= \text{tr} [(X - Z)QZ^H] \\ &= \text{tr} [(XAA^\dagger - ZQ)Z^H] \\ &= \text{tr} [(BA^\dagger - Z)Z^H] \\ &= 0 \end{aligned}$$

Note that Eq. (59) is an inner product corresponding to the Frobenius norm  $\|\cdot\|_F$ . Hence

$$\begin{aligned}\|X\|_F^2 &= \|X - Z\|_F^2 + 2(X - Z, Z)_F + \|Z\|_F^2 \\ &= \|X - Z\|_F^2 + \|Z\|_F^2 \\ &\geq \|Z\|_F^2\end{aligned}$$

with equality if and only if  $X = Z$ .  $\square$

Let  $H' \equiv H - H_{m-1}$ . Thus the optimization problem (24) can be replaced by its equivalent one

$$\begin{cases} \min_{H'} \|H'\|_F^2 \\ \text{s.t. } H'Y_{m-1} = -(S_{m-1} + H_{m-1}Y_{m-1}), \end{cases} \quad (59)$$

It follows from Lemma 1 that the solution to the problem Eq. (59) is

$$H' = -(S_{m-1} + H_{m-1}Y_{m-1}) (Y_{m-1}^T Y_{m-1})^{-1} Y_{m-1}^T. \quad (60)$$

Therefore the solution to the problem (24) is

$$H = H_{m-1} - (S_{m-1} + H_{m-1}Y_{m-1}) (Y_{m-1}^T Y_{m-1})^{-1} Y_{m-1}^T. \quad (61)$$

This work was partially supported by the National Key Research and Development Program of China under Grant 2016YFB0201204, the National Science Foundation of China under Grants 11501039 and 91430218.

---

[1] P. Hohenberg and W. Kohn, Phys. Rev. **136**, B864 (1964), URL <https://link.aps.org/doi/10.1103/PhysRev.136.B864>.

[2] W. Kohn and L. J. Sham, Phys. Rev. **140**, A1133 (1965), URL <https://link.aps.org/doi/10.1103/PhysRev.140.A1133>.

[3] G. Kresse and J. Furthmüller, Phys. Rev. B **54**, 11169 (1996), URL <https://link.aps.org/doi/10.1103/PhysRevB.54.11169>.

[4] G. Kresse and J. Furthmüller, Computational Materials Science **6**, 15 (1996), ISSN 0927-0256, URL <http://www.sciencedirect.com/science/article/pii/0927025696000080>.

[5] J. F. Annett, Computational Materials Science **4**, 23 (1995), ISSN 0927-0256, URL <http://www.sciencedirect.com/science/article/pii/0927025694000133>.

[6] L. D. Marks and D. R. Luke, Phys. Rev. B **78**, 075114 (2008), URL <https://link.aps.org/doi/10.1103/PhysRevB.78.075114>.

[7] P. J. Hasnip, K. Refson, M. I. J. Probert, J. R. Yates, S. J. Clark, and C. J. Pickard, Philosophical Transactions of the Royal Society of London A: Mathematical, Physical and Engineering Sciences **372** (2014), ISSN 1364-503X, <http://rsta.royalsocietypublishing.org/content/372/2011/20130270.full.pdf>, URL <http://rsta.royalsocietypublishing.org/content/372/2011/20130270>.

[8] J. K. Norskov, F. Abild-Pedersen, F. Studt, and T. Bligaard, Proceedings of the National Academy of Sciences **108**, 937 (2011), <http://www.pnas.org/content/108/3/937.full.pdf>, URL <http://www.pnas.org/content/108/3/937.abstract>.

[9] P. Pulay, Chemical Physics Letters **73**, 393 (1980), ISSN 0009-2614, URL <http://www.sciencedirect.com/science/article/pii/0009261480803964>.

[10] C. G. Broyden, Math. Comp. **19**, 577 (1965).

[11] G. P. Kerker, Phys. Rev. B **23**, 3082 (1981), URL <https://link.aps.org/doi/10.1103/PhysRevB.23.3082>.

[12] D. Raczkowski, A. Canning, and L. W. Wang, Phys. Rev. B **64**, 121101 (2001), URL <https://link.aps.org/doi/10.1103/PhysRevB.64.121101>.

[13] D. Vanderbilt and S. G. Louie, Phys. Rev. B **30**, 6118 (1984), URL <https://link.aps.org/doi/10.1103/PhysRevB.30.6118>.

[14] Y. Shiihara, O. Kuwazuru, and N. Yoshikawa, Modelling and Simulation in Materials Science and Engineering **16**, 035004 (2008), URL <http://stacks.iop.org/0965-0393/16/i=3/a=035004>.

[15] L. Lin and C. Yang, SIAM Journal on Scientific Computing **35**, S277 (2013), <http://dx.doi.org/10.1137/120880604>, URL <http://dx.doi.org/10.1137/120880604>.

[16] K.-M. Ho, J. Ihm, and J. D. Joannopoulos, Phys. Rev. B **25**, 4260 (1982), URL <https://link.aps.org/doi/10.1103/PhysRevB.25.4260>.

[17] A. Sawamura and M. Kohyama, Mater. Trans. **45**, 1422 (2004).

[18] P.-M. Anglade and X. Gonze, Phys. Rev. B **78**, 045126 (2008), URL <https://link.aps.org/doi/10.1103/PhysRevB.78.045126>.

[19] R. B. R and R. Ahlrichs, J. Chem. Phys. **104**, 9047 (1996).

[20] D. D. Johnson, Phys. Rev. B **38**, 3082 (1988).

[21] H. Fang and Y. Saad, *Numer. Linear. Algebra Appl.* **16**, 197 (2009).

[22] L. LANDAU and E. LIFSHITZ, *Electrodynamics of Continuous Media (Second Edition Revised and Enlarged)*, vol. 8 (Pergamon, 1984), second edition revised and enlarged ed.

[23] R. Resta, *Phys. Rev. B* **16**, 2717 (1977), URL <https://link.aps.org/doi/10.1103/PhysRevB.16.2717>.

[24] D. R. Penn, *Phys. Rev.* **128**, 2093 (1962), URL <https://link.aps.org/doi/10.1103/PhysRev.128.2093>.

[25] G. Srinivasan, *Phys. Rev.* **178**, 1244 (1969), URL <https://link.aps.org/doi/10.1103/PhysRev.178.1244>.

[26] J. P. Walter and M. L. Cohen, *Phys. Rev. B* **2**, 1821 (1970), URL <https://link.aps.org/doi/10.1103/PhysRevB.2.1821>.

[27] X. S. Shajan and C. Mahadevan, *Crystal Research and Technology* **27**, 253 (1992), ISSN 1521-4079, URL <http://dx.doi.org/10.1002/crat.2170270217>.

[28] P. K. W. Vinsome and D. Richardson, *Journal of Physics C: Solid State Physics* **4**, 2650 (1971), URL <http://stacks.iop.org/0022-3719/4/i=16/a=030>.

[29] J. Fang, X. Gao, H. Song, and H. Wang, *The Journal of Chemical Physics* **144**, 244103 (2016), <http://dx.doi.org/10.1063/1.4954234>, URL <http://dx.doi.org/10.1063/1.4954234>.

[30] X. Gao, Z. Mo, J. Fang, H. Song, and H. Wang, *Computer Physics Communications* **211**, 54 (2017), ISSN 0010-4655, high Performance Computing for Advanced Modeling and Simulation of Materials, URL <http://www.sciencedirect.com/science/article/pii/S0010465516301837>.

[31] Z. Mo, A. Zhang, X. Cao, Q. Liu, X. Xu, H. An, W. Pei, and S. Zhu, *Frontiers of Computer Science in China* **4**, 480 (2010), ISSN 1673-7466, URL <http://dx.doi.org/10.1007/s11704-010-0120-5>.

[32] J. P. Perdew, K. Burke, and M. Ernzerhof, *Phys. Rev. Lett.* **77**, 3865 (1996), URL <https://link.aps.org/doi/10.1103/PhysRevLett.77.3865>.

[33] G. Kresse and D. Joubert, *Phys. Rev. B* **59**, 1758 (1999), URL <https://link.aps.org/doi/10.1103/PhysRevB.59.1758>.

[34] B. Liu, in *Numerical Algorithms in Chemistry: Algebraic Methods*, edited by E. Moler and I. Shavitt (Lawrence Berkley Lab. Univ. of California, 1978), p. 49.

[35] A. Molina-Sánchez and L. Wirtz, *Phys. Rev. B* **84**, 155413 (2011), URL <https://link.aps.org/doi/10.1103/PhysRevB.84.155413>.

[36] T. Cheiwhanchamnangij and W. R. L. Lambrecht, *Phys. Rev. B* **85**, 205302 (2012), URL

<https://link.aps.org/doi/10.1103/PhysRevB.85.205302>.

- [37] L. Liang and V. Meunier, *Nanoscale* **6**, 5394 (2014), URL <http://dx.doi.org/10.1039/C3NR06906K>.
- [38] N. Saigal, V. Sugunakar, and S. Ghosh, *Applied Physics Letters* **108**, 132105 (2016), <http://dx.doi.org/10.1063/1.4945047>, URL <http://dx.doi.org/10.1063/1.4945047>.
- [39] I. Popov, G. Seifert, and D. Tománek, *Phys. Rev. Lett.* **108**, 156802 (2012), URL <http://link.aps.org/doi/10.1103/PhysRevLett.108.156802>.
- [40] Y. Zhou, D. Kiriya, E. E. Haller, J. W. Ager, A. Javey, and D. C. Chrzan, *Phys. Rev. B* **93**, 054106 (2016), URL <https://link.aps.org/doi/10.1103/PhysRevB.93.054106>.
- [41] J. Kang, W. Liu, D. Sarkar, D. Jena, and K. Banerjee, *Phys. Rev. X* **4**, 031005 (2014), URL <https://link.aps.org/doi/10.1103/PhysRevX.4.031005>.
- [42] Strictly speaking, the  $\varepsilon$  derived here is respect to the potential. However, under the condition of homogeneous system, the potential dielectric response function and charge dielectric response function are same. This is because the  $\chi$  in Eq. (15) becomes diagonalized thus the product of  $\chi \cdot U$  equals to  $U \cdot \chi$ .